2012

Potential Energy and Dipole Moment Surfaces of HCO- for the Search of H- in the Interstellar Medium

M. Ayouz
Marquette University

I. Mikhailov
University of Central Florida

Dmitri Babikov
Marquette University, dmitri.babikov@marquette.edu

M. Raoult
Université Paris-Sud

S. Galtier
University of Central Florida

See next page for additional authors

Potential energy and dipole moment surfaces of HCO^- for the search of H^- in the interstellar medium

M. Ayouz,[1] I. Mikhailov,[2] D. Babikov,[1] M. Raoult,[3] S. Galtier,[2,3] O. Dulieu,[3] and V. Kokoouline[2,3,a)]

[1]*Department of Chemistry, Marquette University, P.O. Box 1881, Milwaukee, Wisconsin 53201, USA*
[2]*Department of Physics, University of Central Florida, Orlando, Florida 32816, USA*
[3]*Laboratoire Aimé Cotton, CNRS, Bât. 505, Université Paris-Sud, 91405 Orsay Cedex, France*

(Received 19 December 2011; accepted 16 May 2012; published online 14 June 2012)

Potential energy and permanent dipole moment surfaces of the electronic ground state of formyl negative ion HCO^- are determined for a large number of geometries using the coupled-cluster theory with single and double and perturbative treatment of triple excitations *ab initio* method with a large basis set. The obtained data are used to construct interpolated surfaces, which are extended analytically to the region of large separations between CO and H^- with the multipole expansion approach. We have calculated the energy of the lowest rovibrational levels of HCO^- that should guide the spectroscopic characterization of HCO^- in laboratory experiments. The study can also help to detect HCO^- in the cold and dense regions of the interstellar medium where the anion could be formed through the association of abundant CO with still unobserved H^-. © *2012 American Institute of Physics*. [http://dx.doi.org/10.1063/1.4724096]

I. INTRODUCTION

More than one hundred neutral molecular species have been observed in various regions of the interstellar medium (ISM), while a comparatively low number (about 30) of molecular ion species have been detected up till now. This illustrates the extreme richness and complexity of the interstellar chemistry. Considering the electronic affinity of several neutral molecules present in the ISM, it was speculated for about two decades that molecular negative ions could also be formed in the ISM.[1] This hypothesis has been confirmed in 2006 with the observation of the C_6H^- ion,[2–6] rapidly completed by the discovery of C_4H^-,[7] C_8H^-,[8] C_3N^-,[9] C_5N^-,[3,6] and CN^-.[10] Their formation process is not yet fully understood, and it was suggested that the radiative electron attachment to pre-existing carbon chains is the final step in the formation.[1,4,5]

Besides, the simplest negative ion, H^-, could possibly be formed in a considerable amount by the dissociative attachment of an electron to H_2: $H_2 + e^- \rightarrow H^- + H$. However, H^- has never been detected in the ISM and, therefore, is generally ignored in astrophysical models. Its direct detection is difficult: It has no stable excited bound state,[11] so that its absorption spectrum is featureless in the infrared and visible spectral regions. However, H^- has resonances in the far-ultraviolet region.[11,12] These resonances have been looked for in so-far unsuccessful attempts to detect H^- in the ISM.[13,14]

In our previous study,[15,16] radiative association (RA) of H_2 and H^- yielding the H_3^- ion and a photon was considered as a possibility to probe the presence of H^- in the ISM by detecting rovibrational bound levels of H_3^- via infrared absorption spectroscopy. The potential energy surface (PES) and the permanent dipole moment surfaces (PDMS) of the H_3^- ground state computed in Ref. 15 were used to determine energies of H_3^- rovibrational levels, as well as cross sections and rate constants for the RA process[15] for $T < 100$ K. The rates were found too small (1.6×10^{-23} cm^3/s for *para*-H_2 and 6×10^{-23} cm^3/s for *ortho*-H_2 at 20 K) to produce H_3^- in a significant amount.

Here, we continue to explore the idea of an indirect detection of H^- through its radiative association to a CO molecule (the second most abundant molecule in the ISM) to form the HCO^- ion. The formyl anion has been observed in a flowing afterglow source.[17] Using low-resolution photoelectron spectroscopy,[17] the equilibrium geometry of HCO^- (r_e(CO) $= 2.28 \pm 0.04\ a_0$, r_e(CH)=$2.40 \pm 0.04\ a_0$, $\angle$HCO $= 109 \pm 2°$, where $a_0 = 0.52917721092$ Å is the Bohr radius) as well as the HCO electron affinity 0.313 ± 0.005 eV have been determined. Furthermore, the absence of hot bands in the photoelectron spectrum lead the authors to assume a lower limit of about 800 cm^{-1} on excited vibrational energies of HCO^-. It is worth quoting the warning statement of the authors of Ref. 17: "(given) the rather restrictive assumptions used in this analysis, this geometry should be taken as suggestive, but not unique." On the theoretical side, Tschumper *et al.*[18] determined the equilibrium geometry of HCO^- using various implementations of the density functional theory, and obtained the range of values: $2.326a_0 < r_e(\mathrm{CO}) < 2.366a_0$, $2.288a_0 < r_e(\mathrm{CH}) < 2.398a_0$, $109.8° < \angle\mathrm{HCO} < 110.3°$, as well as harmonic vibrational frequencies. An electron affinity ranging between 0.13 and 0.92 eV was also derived. Note that the HCO^- electron affinity is much smaller than the one (3–4.5 eV) of the carbon-chain anions that have been detected in the ISM.[4,19] It is, however, much higher than the average collision energy in the ISM, which ensures thermal stability for HCO^-.

a)Electronic mail: viatcheslav.kokoouline@ucf.edu.

In the perspective of studying the radiative association of CO with H^-, we performed in this article an accurate *ab initio* calculation of the PES and PDMS of the HCO^- electronic ground state in the chemical range of internuclear distances for several thousands of geometries, and we determined the long-range behavior of the CO–H^- potential energy and dipole moment. We interpolated the obtained PES and PDMS, and prepared a FORTRAN subroutine that evaluates PES and PDMS for any HCO^- geometry. Finally, we calculated the corresponding bound rovibrational levels of the HCO^- molecule. The rest of the article is organized in the following way. In Sec. II, we describe the performed *ab initio* calculations (AIC). In Sec. III, we present the procedure for the interpolation of the obtained PES. Section IV is devoted to the calculation and interpolation of PDMS. Finally, atomic units (a_0) for distances will be used throughout the article.

II. *AB INITIO* CALCULATION OF THE HCO^- GROUND STATE POTENTIAL ENERGY SURFACE

We employed the coupled-cluster theory with single and double and perturbative treatment of triple excitations method (CCSD(T)), which is part of the GAUSSIAN 09 Revision A.02 package of *ab initio* programs.[20] In the calculation, we used the polarized valence quadrupole-zeta correlation consistent basis set `d-aug-cc-pVQZ` augmented with two diffuse functions of each symmetry: *spdf*-orbitals for hydrogen and *spdfg*-orbitals for oxygen and carbon. Thus, our contracted basis set is [7*s*6*p*5*d*4*f*3*g*/6*s*5*p*4*d*3*f*]. Scuseria *et al.*,[21] who used CCSD(T)/[10*s*9*p*4*d*2*f*1*g*] demonstrated that triple excitations as well as *g*-type functions in the basis set are crucial in the calculation of CO dipole moment to obtain satisfactory agreement with experiment. The choice of the *ab initio* method and of the basis set was made after preliminary benchmark calculations of the H^- energy. The use of a large basis set augmented with diffuse orbitals is important to properly describe the diffuse electronic cloud of the negative ion. The hydrogen affinity is smaller by only 2 cm^{-1} compared to the experimental value.[22] The equilibrium distance, dipole moment as well as the well depth of the CO ground electronic state (see Table I) are in good agreement with the previous accurate *ab initio* results of Refs. 21 and 23. The accuracy of the present HCO^- calculations can also be assessed comparing the numerical and analytical behavior of the CO + H^- energies and PDMS for large separations between CO and H^- as discussed in Secs. III and IV. We have decided not to increase further the basis set because the calculation would become too long to perform for several thousands geometries. Evaluating the interaction energy, we have ignored the basis set superposition error using the counterpoise correction procedure of Boys and Bernardi[24] because without a systematic analysis of basis set convergence the correction may cause even large error in the interaction energy.[25]

As in the study of H_3^-,[15] we used the Jacobi coordinates, r, R, γ: r is the distance between C and O, R is the distance from the center of mass of CO to H, and γ is the angle between vectors $\vec{R}$ and $\vec{r}$. The grid in r is uniform from $r = 1.7a_0$ to $r = 2.9a_0$ with step $\Delta r = 0.1\ a_0$; in addition, points with $r = 1.5a_0$ have also been included in the grid in order to represent the strongly repulsive character of the potential for small distances r. The grid in γ changes from 0° to 180° by a constant step of $\Delta\gamma = 18°$. The grid in R is dense at small R and sparse at large R according to the formula $R_i = 1.4 + 0.4\exp(i/10)$ (in a_0) with $i = 0, 1, \ldots, 49$, which makes R changing from 1.80 to 55.116 a_0. Therefore, the calculations were performed for $13 \times 11 \times 50 = 7150$ geometries.

TABLE I. Summary of HCO^- PES properties: *a*–asymptotic energy at infinite separation between CO and H^-; *b*–the value obtained using the 3D B-spline interpolation procedure (based on CCSD(T) energies) discussed in the text; *cc*–the value from the CCSD(T) optimization; *ca*–the value from the CASSCF optimization; *ci*–the value from the MRCI/CASSCF optimization; *d*–energy of the global PES minimum, GM in Fig. 8; *e*–previous calculation[18]; *f*–experiment;[17] *g*–energy of the maximum of the reef in Fig. 8; *h*–energy of the second PES minimum, LM in Fig. 8; *i*–the CO equilibrium distance; *k*–obtained by scan along r with step 2×10^{-4}; *l*–experiment[29]; *m*–CCSD(T)/[10*s*9*p*4*d*2*f*1*g*] calculation;[21] *n*–CO dipole moment at r_e; *o*–CO dipole moment at experimental value of $r_e = 2.132221$; *p*–energy of H^- obtained by adding 0.5 hartree to the experimental affinity[22] of H^-. The distances are in a_0, angles are in degrees.

Quantity	This study	Other Refs.
$D_{as}(r = 2.138)^a$	$-113.718\ 283^b$,	
(hartree)	$-113.718\ 242^{cc}$	
GM[d] (hartree)	$-113.728\ 934^b$	
Position of GM:		
R	3.08^b, 3.02^{cc}, 3.04^{ca}	
γ	134.1^b, 134.5^{cc}, 135.3^{ca}	
r_{CO}	2.33^b, 2.34^{cc}, 2.34^{ca}	$2.33–2.37^e$, 2.29^f
r_{CH}	2.36^b, 2.29^{cc}, 2.29^{ca}	$2.29–2.39^e$, 2.40^f
∠HCO	110.2^b, 109.9^{cc}, 111.2^{ca}	$109.8–110.3^e$, 109^f
Reef position: r, R, γ	2.20^b, 4.27^b, 123.8^b	
Position of LM		
R	6.02^b, 6.92^{ca}	
γ	110.0^b, 100.5^{ca}	
r	2.15^b, 2.14^{ca}	
D_{as} − GM (cm^{-1})	2338^b, 2484^{ci}	
D_{as} −reef (cm^{-1})	287.2^b	
D_{as} − LM (cm^{-1})	685^b, 643^{ci}	
Properties obtained separately for CO and H^-		
$r_e(CO)^i$	2.1388^k	2.132221^l, 2.1316^m
$d(r_e)^n$ (ea_0)	0.0417, 0.0462^o	0.0484^l, 0.0492^m
$E_{CO}(r_e)$ (hartree)	$-113.190\ 780$	
E_{H^-} (hartree)	$-0.527\ 463$	$0.527\ 716^p$
$E_{CO}(r_e) + E_{H^-}$ (hartree)	113.718 243	

For some geometries of the grid defined above, the ground electronic state of HCO^- does not converge. This occurs when the HCO^- PES is close to and crosses the HCO PES so that the energy of the electronic state of HCO^- goes from the discrete spectrum to the continuum. It happens near the HCO equilibrium geometry. We found the HCO equilibrium geometry at $r = 2.2a_0$, $R = 3.0a_0$, $\gamma = 144°$, in reasonable agreement with the accurate values of Ref. 26. The autodetachment region occurs at energies about 7000 cm^{-1} above the H^- + CO dissociation limit, such that the autodetachment will have a negligible effect in the calculation of HCO^- bound levels and CO + H^- continuum states at small kinetic energies. Nevertheless, we decided to define the PES over the entire grid to use the PES in other types of coordinates like the hyper-spherical ones, as it is done, for example,

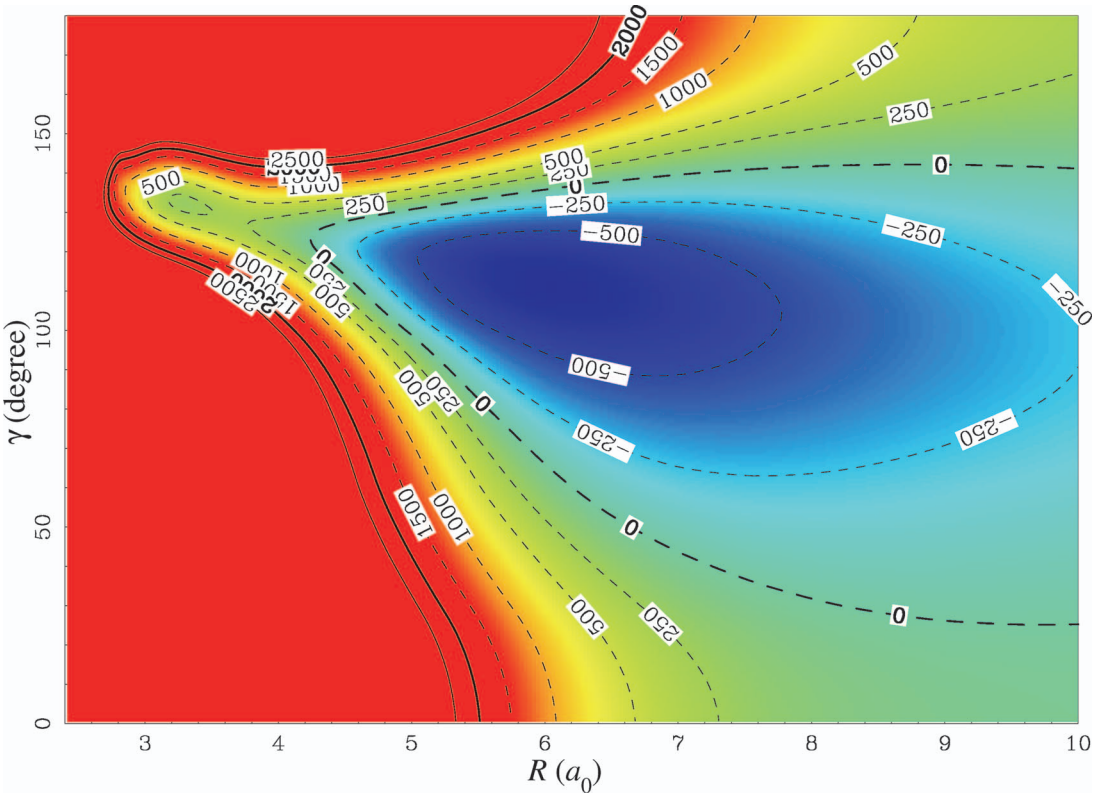

FIG. 1. The HCO^- potential energy surface for a fixed value $r = 2.15a_0$ as a function of R and γ. The numbers on the contour plot lines label the PES energy in cm^{-1}. The value $r = 2.15a_0$ is close to the equilibrium position of CO molecule and corresponds to the local minimum of the long-range potential of interaction between CO and H^-, see local minimum (LM) in Table I.

in Ref. 15. We extended the PES in the autodetachment region, with a 3D interpolation procedure that uses converged geometries as interpolation knots and interpolate the PES at missing geometries. For this purpose, we used the fitting approach of Braams and Bowman.[27]

Figures 1–3 illustrate the HCO^- PES in Jacobi coordinates for three values of $r = 2.15$, 2.2, and $2.33a_0$, respectively. The origin of potential energy in the figures is shifted to the energy of the CO molecule at the equilibrium position r_e(CO) with the H^- ion at the infinite separation from CO.

When the distance between CO and H^- is very large ($>200a_0$), the minimum of PES corresponds to $\gamma = 0$ with r equal to the equilibrium distance of the free CO molecule as a result of the H^-–CO charge-dipole interaction. At values of R between 8 and $150a_0$, the charge-quadrupole interaction is dominant over the charge-dipole interaction (because the dipole moment of CO at equilibrium is small, 0.05 ea_0 compared to the quadrupole moment of $-1.5\ ea_0^2$), shifting the PES minimum gradually from $\gamma = 0$ towards 90° as R decreases (see Fig. 1). At distances near $R \sim 10a_0$, the PES is lower for larger values of r because the CO dipole moment grows with r (with the sign opposite to one at the CO equilibrium value). Additional interaction energy due to the charge-dipole interaction shifts the position of the PES minimum along γ to even larger angles γ, as seen in Fig. 2. At the same time, at such large distances r, the second potential well occurs in the chemical interaction region. Finally, the global minimum is formed at $R = 3.08, r = 2.33, \gamma = 134.1°$ (Fig. 3).

A similar behavior was observed for the HCO molecule,[26] for which PES changes its character near the geometry $r_{CO} = 2.2a_0$ and $r_{CH} = 2.4a_0$, where two electronic configurations of the A' symmetry are mixed together. At the linear geometry of the HCO molecule, the two configurations become $^2\Sigma^+$ and $^2\Pi$ states, and at a large separation between CO and H, they correlate with the $^1\Sigma^+$ and $^3\Pi$ states of the CO molecule. In the present case of the HCO^- molecule, the two configurations mixed near $r = 2.1a_0$ and $R = 3a_0$ correlate at large R with the CO($^1\Sigma^+$)+H^- channel and the three-body fragmentation channel CO($^1\Sigma^+$) + H + e^- located below the CO($^3\Pi$) + H^- dissociation energy.

To benchmark our CCSD(T) results, we have made limited calculations using the multi-reference configuration interaction (MRCI) and complete active space self-consistent field (CASSCF) methods with the same basis set `d-aug-cc-pVQZ` reduced to *spdf*-orbitals for all atoms. These computations were done with the MOLPRO[28] suite of programs. We have included 12 electrons and 16 Hartree-Fock orbitals (14 a' and 2 a'') in the active space. Including higher orbitals, we have verified that this level of theory provides energy converging to a few cm^{-1}. Using the CASSCF method we have found positions of the two minima of the HCO^- PES. The positions agree well with those obtained by CCSD(T) as shown in Table I. Single-point MRCI calculations have been performed using 12 a' and 2 a'' CAS orbitals and correlating 12 electrons. The Davidson correction has been included in final energy values. We have estimated convergence of this MRCI/CASSCF method about 50 cm^{-1}.

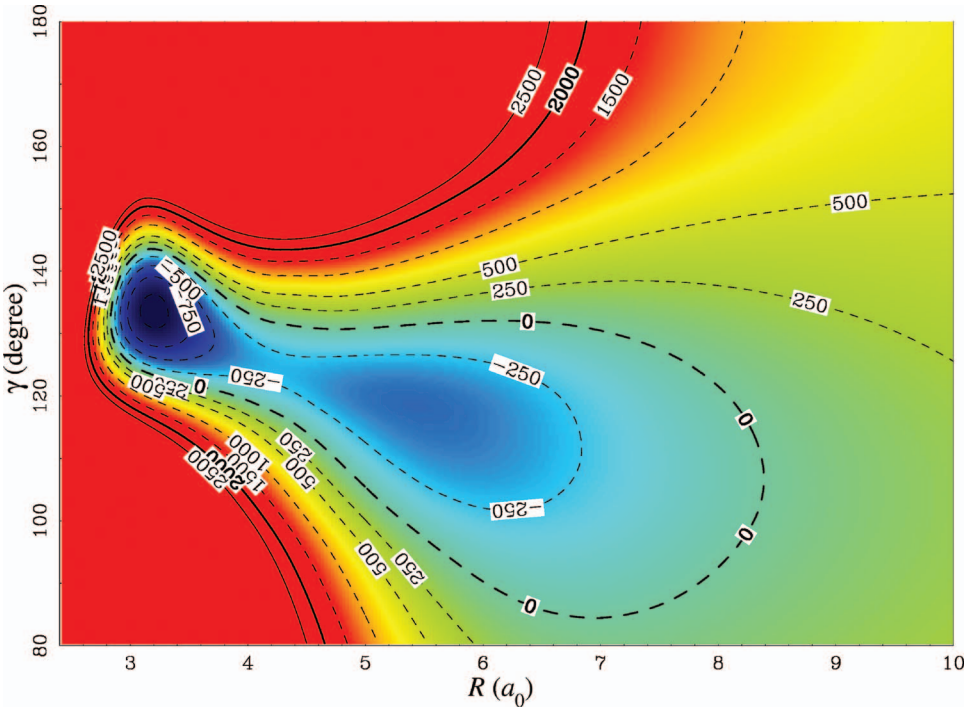

FIG. 2. Same as Fig. 1 except $r = 2.2a_0$. For this value of r, the HCO^- potential has two separated potential wells, one is at large distances, the second one is at small distances between CO and H^-.

Using the MRCI/CASSCF method we have obtained the dissociation energy for the two minima optimized with CASSCF: 2484 cm^{-1} (inner potential well) and 643 cm^{-1} (outer potential well). They agree well with the CCSD(T) results, 2338 cm^{-1} and 685 cm^{-1}, respectively (see Table I). Using the MRCI/CASSCF method, we have also determined the geometry minimum of the HCO PES ($R = 3.09a_0, r = 2.15a_0, \gamma = 143.4°$), the HCO equilibrium dissociation energy of 6633 cm^{-1}, and the HCO zero-point energy of 2789 cm^{-1} in the normal mode approximation. Our results agree well with the previous calculation by Werner *et al.*,[26] who obtained geometry of the minimum $R = 3.02a_0$, $r = 2.23a_0, \gamma = 144.9°$; the dissociation energy of 6340 cm^{-1}; and the zero-point energy of 2895 cm^{-1} (obtained by

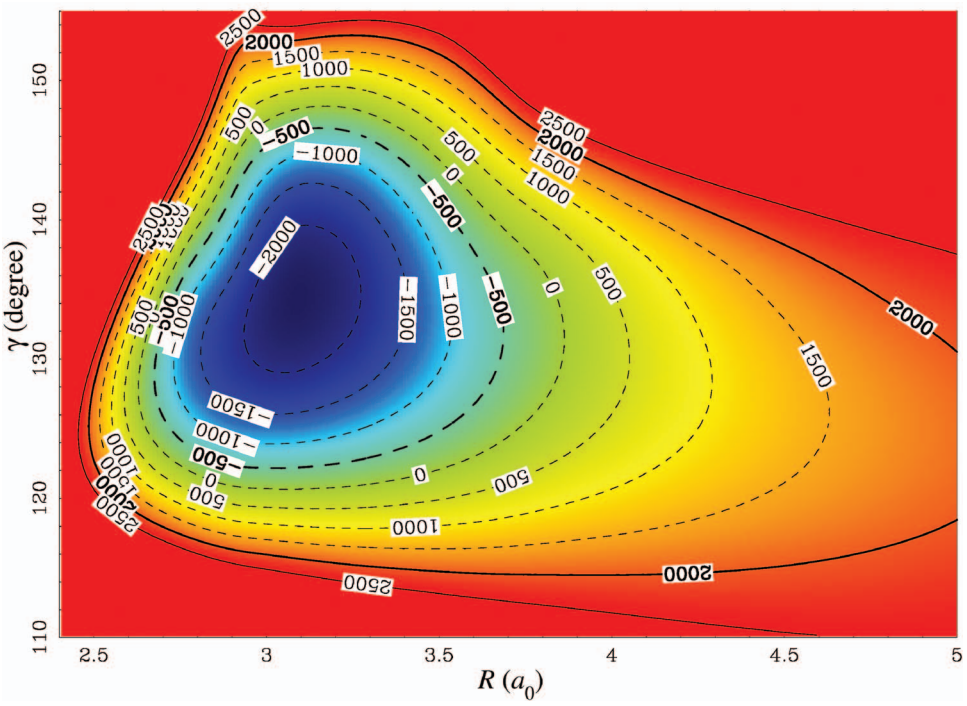

FIG. 3. Same as Fig. 1 except $r = 2.33a_0$. This value of r corresponds to the global minimum (GM) of the potential (see Table I).

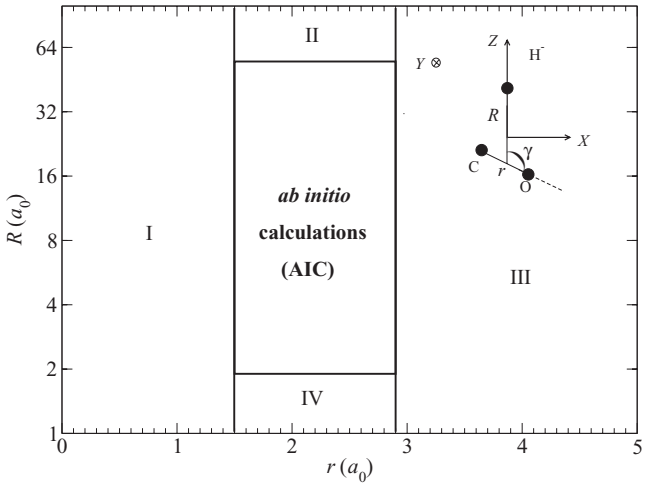

FIG. 4. The five regions of configuration space in Jacobi coordinates R, r defined for the PES calculations, for all values of γ. Notice that R is given in a logarithmic scale. The region of AIC is extended to regions I–IV where the PES is extrapolated.

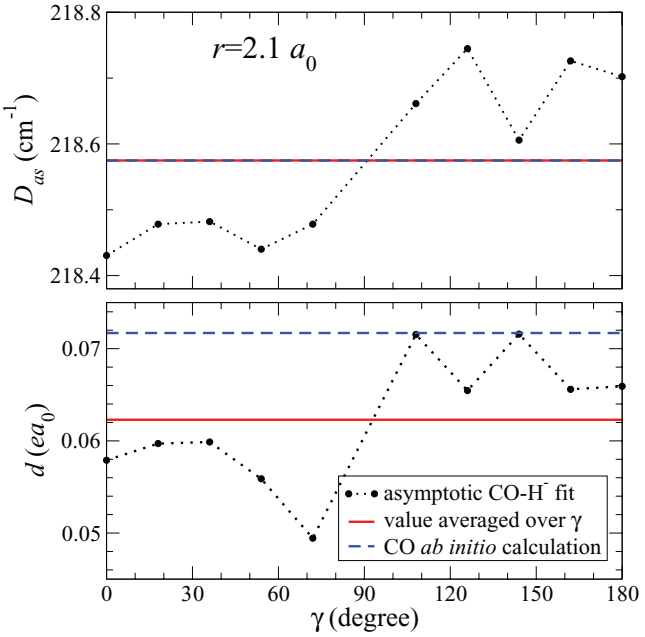

FIG. 5. Parameters D_{as} and d of Eq. (1) obtained from the asymptotic behavior of the present CO−H$^-$ PES and compared to the *ab initio* values obtained for the CO molecule alone. The results are shown only for $r = 2.1a_0$. The γ-dependence of the fitted values of D_{as} and d is attributed to the higher order terms in the asymptotic expansion of Eq. (1). Because D_{as} and d in Eq. (1) should not depend on γ when the global PES is extended beyond the grid of *ab initio* geometries, we use γ-independent values for D_{as} and d (red curves in the figure), which are obtained by averaging the fitted values over γ. To make a smooth transition between the *ab initio* energies and asymptotic energies beyond the *ab initio* geometries, we allow the parameter q_{zz} to be γ-dependent (see Fig. 6).

diagonalization of the vibrational Hamiltonian, not in the normal mode approximation).

III. INTERPOLATION AND LONG-RANGE BEHAVIOR OF THE HCO$^-$ GROUND STATE POTENTIAL SURFACE

For the bound state calculations, and in view of future scattering calculations for H$^-$−CO radiative association, the PES is interpolated in the region of calculated *ab initio* energies similarly to our previous study of H_3^-.[15,16] Outside this region the PES is calculated using analytical formulas. We divided the $r \times R$ configuration space in five different parts: the region of AIC and four regions (I–IV) surrounding AIC (see Fig. 4). Regions AIC and II are the only ones relevant to bound and scattering states of the H$^-$ + CO system with energies below the autodetachment threshold.

Inside the three-dimensional box $r \in [1.5a_0;\ 2.9a_0]$, $R \in [1.80a_0; 55.116a_0]$, $\gamma \in [0; 180^\circ]$ (AIC in Fig. 4), a three-dimensional B-spline interpolation procedure is employed. Wave functions of bound and continuum states at low energies vanish in regions I, III, and IV, so some convenient analytical formulas can be used in these regions. The formulas should only ensure (1) a smooth transition across the boundaries between the regions (especially boundaries with regions AIC and II), and (2) large values of PES to prevent a non-negligible probability density in these regions.

In region II, we describe the long-range (as a function of R, at fixed r and γ) potential V_{LR} for the interaction between CO and H$^-$ by the two dominant terms of the multipole expansion: the dipole-charge and quadrupole-charge interactions,

$$V_{LR}(R;r,\gamma) = D_{as}(r) + \frac{C_2}{R^2} + \frac{C_3}{R^3} \text{ with}$$
$$C_2 = -d(r)P_1(\cos\gamma) \text{ and}$$
$$C_3 = -q_{zz}(r)P_2(\cos\gamma)/2. \qquad (1)$$

The first term $D_{as}(r)$ is the sum of H$^-$ and CO(r) energies at a given internuclear distance r of the CO molecule. The second and third terms are the charge-dipole and charge-quadrupole interactions between H$^-$ and CO. P_1 and P_2 are the first and second order Legendre polynomials. To avoid any confusion about the definition of $q_{zz}(r)$ used here, we give the explicit formula for the corresponding operator $\hat{q}_{zz} = \sum_q q(3\hat{z}_q^2 - \hat{r}_q^2)$, where the sum is evaluated over all charges q in the CO molecule, $\hat{r}_q$ and $\hat{z}_q$ refer to coordinates of the charges with the z axis along the CO axis.

The coefficients $d(r)$ and $q_{zz}(r)$ are obtained from the present *ab initio* calculations in the following way. First, for each r and γ, values of D_{as}, d, and q_{zz} are obtained numerically using Eq. (1) and the last three *ab initio* points ($R = 45.379a_0, 50.004a_0$, and $55.116a_0$) along R for given r and γ. The obtained quantities D_{as}, d, and q_{zz} are consistent with accurate *ab initio* calculations made separately for CO[29,30] (see Figs. 5 and 6). In the asymptotic region they should not depend on γ; their observed weak dependence on γ is due to higher order multipole terms neglected in Eq. (1) and to the employed fitting procedure. In order to avoid using γ-dependent values of D_{as} and d, we average D_{as} and d over γ and use the averaged values $D_{as}(r)$ and $d(r)$ in Eq. (1) beyond $R = 55.116a_0$.

The procedure above determines only $D_{as}(r)$ and $d(r)$, but not $q_{zz}(r)$. In order to ensure continuity of the PES across the $R = 55.116a_0$ boundary, we use γ-dependent functions for

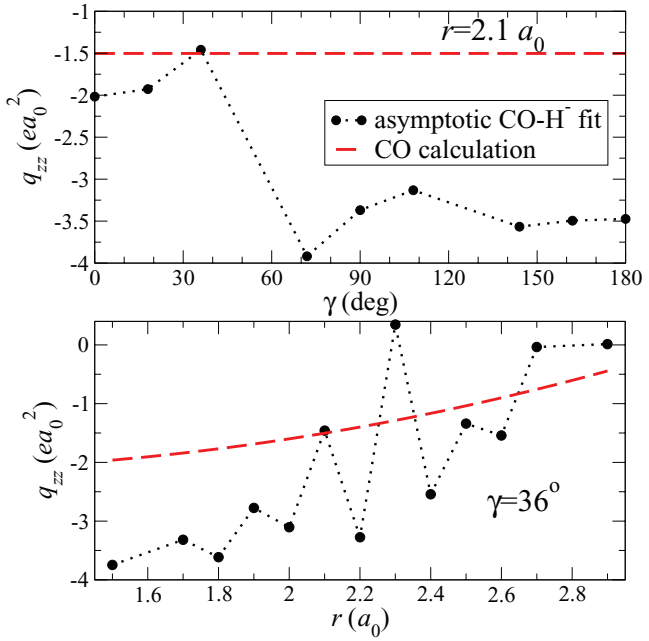

FIG. 6. Two examples of the γ- and r-dependence of the quadrupole moment q_{zz} obtained by fitting the *ab initio* energies to Eq. (1), where D_{as} and d are taken to be γ-independent as discussed in the text. Red curves in the two panels show values obtained in accurate *ab initio* CO calculation.[30] The difference of q_{zz} values obtained by fitting the HCO^- energies from the values obtained in the CO calculation should be attributed to higher order terms that are not accounted in the multipole expansion. The largest contribution that is not explicitly accounted by Eq. (1) is due to the interaction of induced dipole of CO with the charge of H^-. It varies with R as C_4/R^4 and contributes about 0.5 cm^{-1} at $R = 50a_0$.

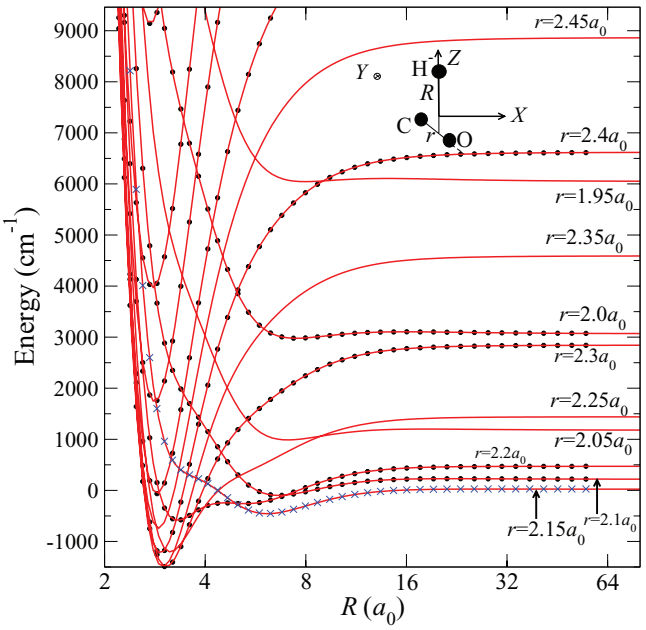

FIG. 7. PES cuts as a function of R at the *ab initio* grid points (r =2.0, 2.1, 2.2, 2.3, and 2.4a_0) and at intermediate points (r =1.95, 2.05, 2.15, 2.25, 2.35, and 2.45a_0), for which energy is obtained by the interpolation procedure. Circles represent the *ab initio* energies used to obtain interpolation coefficients. Crosses on the $r = 2.15a_0$ curve are *ab initio* energies not included in the grid used for interpolation. They are used to verify the quality of the interpolation procedure.

q_{zz}. Therefore, the function $q_{zz}(r, \gamma)$ is obtained from *ab initio* energies using Eq. (1) one more time; but now, the values D_{as} and d are fixed, such that only one point along R ($R = 55.116a_0$) is needed to find $q_{zz}(r, \gamma)$. In this way we obtain function $V(R, r, \gamma)$ that changes continuously across the boundary between regions II and AIC and behaves asymptotically according to Eq. (1) with an "effective" quadrupole moment $q_{zz}(r, \gamma)$. The "effective" quadrupole moment includes the actual γ-independent quadrupole moment and accounts for higher order terms in the asymptotic multipole expansion, such as the interaction between the charge of H^- and induced dipole or octopole of CO ($\sim 1/R^4$) and others.

The analytical extrapolation of PES into the three other regions (I, III, and IV) was made as in Ref. 15. In regions I and IV, we use the following extrapolation formula in r for fixed R and γ:

$$V_{SR}(r; R, \gamma) = a(R, \gamma)e^{-b(R,\gamma)r}, \quad (2)$$

where $a(R, \gamma)$ and $b(R, \gamma)$ are functions of R and γ that are obtained considering the two *ab initio* energies near the corresponding boundary. For regions I or IV, the functions $a(R, \gamma)$ and $b(R, \gamma)$ are obviously different. In a similar way, in region III, we extrapolate the PES along r and at fixed R and γ using a dispersion-like expression,

$$V_{LR}(r; R, \gamma) = D_0(R, \gamma) - \frac{C_6(R, \gamma)}{r^6}, \quad (3)$$

where the $D_0(R, \gamma)$ and $C_6(R, \gamma)$ (always positive) coefficients are obtained in the same way as the coefficients a and b, considering the two *ab initio* grid points near the boundary between regions III and AIC.

Figure 7 demonstrates the result of the interpolation procedure. It shows the potential energy as a function of R for several values of r included in the initial grid of *ab initio* energies as well as for intermediate values of r, which are not included in the grid of *ab initio* geometries. For an additional check of the quality of the interpolation procedure, we calculated *ab initio* energies of several geometries not included in the grid used to build the interpolation coefficients. This additional *ab initio* energies are shown in Fig. 7 by crosses ($r = 2.15a_0$). Interpolated values agree well with the additional energies obtained *ab initio*.

Figure 8 shows the interpolated PES in a different way, as the minimum energy path (MEP) along R: For each given R, a PES minimum is obtained and shown in the figure. The probability density is expected to be maximum near geometries along MEP. The minimum of the curve corresponds to the PES GM. The energy of GM is 2337 cm^{-1} below the H^- + CO(r_e) dissociation limit D_{as}. The curve has a second minimum (LM), which appears near $R = 6\ a_0$ with energy of 685 cm^{-1} below D_{as} and a reef with its maximum located 287 cm^{-1} below D_{as}. The double-well structure of MEP can be considered as a signature of a modification in the electronic configuration of the HCO^- ion when H^- approaches to CO from infinity as discussed at the end of Sec. II. The upper curves of Fig. 8 show the r- and γ-behavior along MEP. The geometries and energies of the reef, GM, and LM are reported

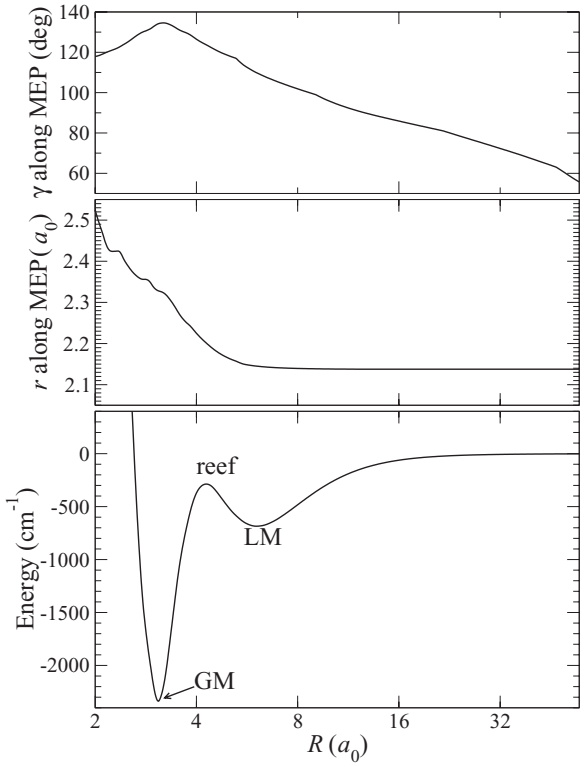

FIG. 8. The minimum energy path (lowest panel) of the PES along the R coordinate. The two upper panels give the r and γ values corresponding to the PES minimum at a given value R. The absolute energy minimum is indicated by GM, the top of potential energy bump is labeled with reef and the second minimum around $R = 6a_0$ is called LM (local minimum).

in Table I, together with other characteristic parameters of the obtained PES.

The position of GM has been previously determined experimentally[17] and theoretically[18] using the density functional theory (Table I). The coordinates from the previous theoretical study are specified by a range of values because different types of functionals have been used in Ref. 18 that gave slightly different values for GM.

The obtained *ab initio* data were used to prepare a FORTRAN subroutine that calculates potential energy for an arbitrary geometry, which is available as a supplementary material.

Using the HCO^- PES, we have calculated energies of several rovibrational levels for two values of the total angular momentum $J = 0$, 1 (Table II) using the same close-coupling method as in the previous study of H_3^-.[16] The details can be found in Refs. 16, 31, and 32. Wave functions of certain levels are primarily localized in the inner potential well. These levels are marked with a star in Table II. The rotational constants, estimated from the energy difference between the $J = 0$ and 1 levels, are considerably larger than those of the other levels localized in the outer well of PES. For each level in the table, we specify only the total angular momentum J and the overall symmetry of the state. In principle, for levels localized in the outer potential well it is possible to assign approximate quantum numbers corresponding to the vibrational excitation of the CO dimer and the projection of the angular momentum on the molecular Z axis, similarly to the H_3^- study.[16] However, this analysis has not been made for HCO^-.

TABLE II. Binding energies of rovibrational levels of the HCO^- ground electronic state. Energies are given in cm^{-1} with respect to the energy D_0^0 of the lowest dissociation limit CO($v = 0$, $j = 0$)+H^-. States with $J = 0$ can only be of the A' irreducible representation. The $J = 1$ states could be of the A' or A'' irreducible representation, but the $J = 1$, A' states have not been calculated. The obtained energies are combined in rotational triads corresponding to the same vibrational excitation. The levels marked with a star are localized primarily in the inner potential well.

$J = 0, A'$	$J = 1, A''$		$J = 0, A'$	$J = 1, A'$	
* −1338.4	* − 1335.7	* − 1324.4	− 97.5	− 95.8	− 94.5
−542.1	− 539.9	− 538.5	− 90.8	− 89.1	− 87.7
−423.9	− 421.7	− 420.6	− 65.7	− 64.2	− 62.6
−366.9	− 364.9	− 363.5	− 63.2	− 61.7	− 60.0
−323.9	− 321.5	− 320.0	− 52.6	− 51.1	− 49.2
* −295.3	* − 290.7	* − 280.4	− 41.5	− 40.1	− 38.3
−272.3	− 270.1	− 268.1	− 39.2	− 37.6	− 35.8
−231.8	− 229.0	− 226.6	− 29.4	− 28.4	− 26.4
−227.9	− 226.0	− 224.6	− 20.4	− 19.2	− 17.0
* − 220.7	* − 214.7	* − 190.6	− 16.6	− 15.4	− 12.7
−190.2	− 188.1	− 186.9	− 13.4	− 12.0	− 10.0
−156.2	− 154.2	153.1	− 6.7	− 6.1	− 3.3
−154.4	− 152.5	151.3	− 3.7	− 3.0	− 1.0
−121.1	− 119.5	− 118.1	− 1.3	− 0.15	
−119.8	− 117.9	− 116.7			

Inspecting the energy spacing between the levels, we deduce that two potential wells are highly an-harmonic. It means that the normal mode analysis cannot produce realistic energy spectrum even for the lowest levels. Indeed, the previous theoretical study of HCO^- of Ref. 18 gave the intervals for the three normal mode frequencies: 1649–1938, 1199–1344, and 1344–1525 cm^{-1}, which are considerably larger than the splitting of 780–800 cm^{-1} between the lowest vibrational levels obtained in our study. It is worth mentioning that the experimental lower-bound estimate for the splitting between the lowest vibrational levels of HCO^- is 800 cm^{-1},[17] which is consistent with our results.

The affinity $A(HCO^-)$ of the lowest HCO^- vibrational level was obtained from the dissociation energy $D_0^0(CO+H)$ = 4600 cm^{-1} of HCO (Ref. 26) and the affinity $A(H^-)$ = 6050 cm^{-1} of H^-: $A(HCO^-) = A(H^-) - D_0^0(CO + H) + D_0^0(CO + H^-) \sim 2790$ cm^{-1}. Because we have determined the interaction energy of the HCO molecule at its equilibrium position, the zero-point energy of HCO, as well as the interaction energy of HCO^- at equilibrium using the MRCI/CASSCF method, we can also calculate the affinity independently of Ref. 26. Using our MRCI/CASSCF data, the zero-point energy of HCO^- from Table II and the experimental affinity of H^-, we obtained the affinity of 2651 cm^{-1}. The difference between the two values (2790 and 2651 cm^{-1}) of the HCO^- affinity provides an order of magnitude of the theoretical precision, which is about 150 cm^{-1}. The obtained affinity is in good agreement with the experimental value 2520± 40 cm^{-1} of Ref. 17.

IV. DIPOLE MOMENT SURFACES

For determination of the cross section for the radiative association between CO and H^-, components of permanent dipole moment are also needed. The two non-zero PDMS-components along X and Z axes have been calculated at the same grid of geometries using the same basis set.

Accuracy of dipole moments needed to compute transition probabilities is less critical than the one required for energies to determine transition frequencies. Therefore, in order to save computing time, we restricted the calculation of the PDMS at the Hartree-Fock (HF) level. The level of theory is benchmarked by comparison of the HF values computed at $\gamma = 90^\circ$ of the PDMS in the asymptotic region (namely, for large R) with the CCSD(T) value[29] of the CO dipole moment: For CO internuclear distances changing between 1.5 a_0 and 2.7 a_0, the HF values of the D_x component of HCO^- (for $\gamma = 90^\circ$) are varying between 0.43 ea_0 and -0.72 ea_0; the CCSD(T) dipole moment of CO is varying between 0.43 ea_0 and -0.31 ea_0. The asymptotic value of the D_Z component of HCO^- can be compared with the expected theoretical value $D_Z = -\frac{m_{CO}}{m_{CO}+m_{H^-}} eR = -0.965517eR$. As illustrated in the upper panel of Fig. 9, the HF value of D_Z obeys the linear variation, with a slope -0.96553 derived from a numerical fit. At short R distances the value of D_Z is certainly less accurate. To give an idea about accuracy of the HF dipole moments at small values of R, we have calculated both components of dipole moment using the CCSD(T) method and the same basis

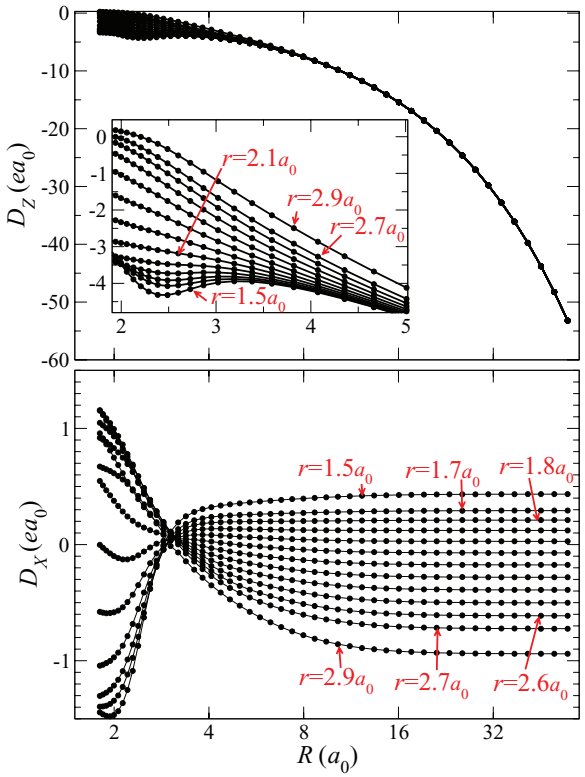

FIG. 9. The two components of the permanent dipole moment for $\gamma = 90^\circ$ for all grid points r. The inset in the upper panel shows a zoom of the Z-component in the region of small values of R. Asymptotically, D_Z varies as $-0.965517R$. At $\gamma = 90^\circ$ and $R \to \infty$, D_X becomes constant and equal to the dipole moment of CO. Notice the logarithmic scale in R.

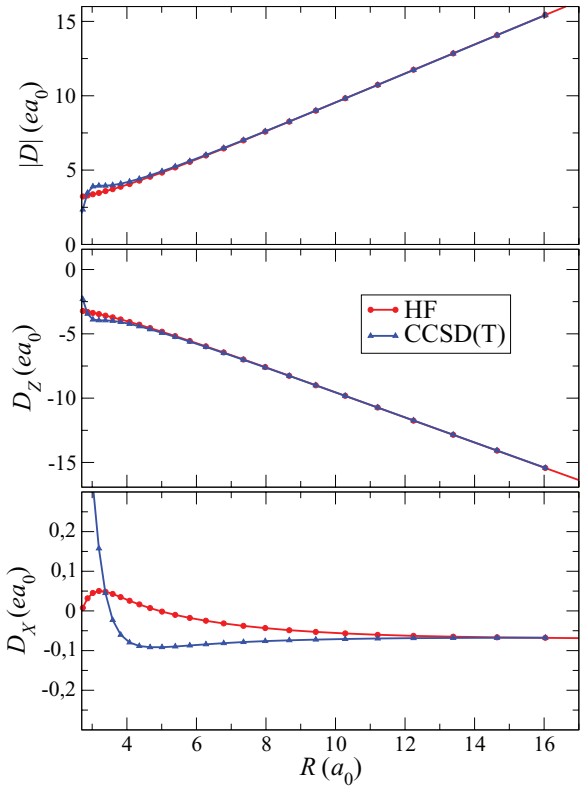

FIG. 10. Absolute values (upper panel) and the two components (two lower panels) of the electric dipole moment of HCO^- obtained using the Hartree-Fock and CCSD(T) methods with the `d-aug-cc-pVQZ` basis. In this calculation, $r = 2.1a_0$ and $\gamma = 90^\circ$.

`d-aug-cc-pVQZ`. The components of dipole moment have been obtained by numerical differentiation of total CCSD(T) energy with respect to a finite external electric field. For each geometry point a total of three calculations in each of the two directions with field strengths 0 and $\pm 10^{-3}$ a.u. were employed. The results are shown in Fig. 10. In the future calculation of the radiative association cross section, accuracy in determination of the cross section will be of the order of one percent or better, because the major contribution to the Franck-Condon factor will be given by geometries $5a_0 < R < 15a_0$. This level of accuracy is satisfactory for cross section calculations.

Similarly to Ref. 15, the obtained *ab initio* PDMS components have been used to prepare a FORTRAN subroutine, which determines the two PDMS components for an arbitrary geometry given by R, r, and γ. In this subroutine, for the central region of Fig. 4, the surfaces are interpolated using the 3D B-splines. At large R (region II in Fig. 4), the D_Z PDMS component behaves linearly with R: $D_Z = -0.965517\,eR$ for all γ and r. The D_X component behaves as $D_X = d(r)\sin(\gamma)$, when $R \to \infty$. In regions I, III, and IV, same empirical formulas as in Ref. 15 are used.

V. CONCLUSION AND PROSPECTS

In this work, we have determined, for the first time, the global potential energy surface of the ground state of the formyl anion HCO^- using a large basis set in the framework of the CCSD(T) method implemented in the GAUSSIAN

package. Using the obtained *ab initio* energies and the multipole expansion at large distances between H^- and CO, we elaborated a FORTRAN interpolation routine (provided as supplementary material)[34] that can be used to obtain potential energy of HCO^- for any geometry. The minimum energy path along the distance between H^- and the CO center-of-mass reveals that the vibrational motion takes place within a double-well structure of the potential energy surface. Two kinds of bound levels are clearly identified, with radial wave functions being localized mostly inside the internal well, or spread over the two wells. The electron affinity of HCO^- obtained in this study, 2650 ± 150 cm^{-1} (the MRCI value) is in good agreement with the experimental value 2520 ± 40 cm^{-1}.[17]

The calculated surfaces of the two components of the dipole moment of HCO^- can be used to obtain the cross section for radiative association between CO and H^- and oscillator strengths for rovibrational transitions in HCO^-. The process of radiative association could be important for the probe of presence of H^- in the ISM: It has been shown in the previous study[16] that the cross section for RA between H^- and H_2 is too small to expect significant amounts of stable H_3^- ions that could be detected through absorption spectroscopy. The CO molecule is the second (after H_2) most abundant molecule in the ISM, and at large distances it has a stronger interaction with H^- compared to H_2. Therefore, we expect the RA cross-section for $CO + H^-$ to be significantly larger than that in the case of $H_2 + H^-$. For detection in the ISM, one could use pure-rotational transitions for the ground vibrational level and rovibrational transitions between excited vibrational levels of HCO^-. Wavelengths for such transitions fall into the sensitivity bands of the Herschel space observatory. These calculations are currently in progress in our group. The computed energy levels of HCO^- as well as RA rates could also be of great help for experiments aiming at studying collisions between neutral molecular species and negative ions in multipole traps.[33]

ACKNOWLEDGMENTS

The study was partially supported by the *Réseau thématique de recherches avancées "Triangle de la Physique,"* Contract No. QCCM-2008-007T; the National Science Foundation (NSF) with Grant No. PHY-1068785, the (U.S.) Air Force Office of Scientific Research (USAFOSR), Grant No. FA9550-09-1-0604. We used resources of "Grappe Massivement Parallèle de Calcul Scientifique de la Fédération Lumière et Matière d'Orsay" and as well the resources of the National Energy Research Scientific Computing Center, which is supported by the Office of Science of the (U.S.) Department of Energy (DOE) under Contract No. DE-AC02-05CH11231.

[1] E. Herbst, Nature (London) **289**, 656 (1981).
[2] M. C. McCarthy, C. A. Gottlieb, H. Gupta, and P. Thaddeus, Astrophys. J. Lett. **652**, L141 (2006).
[3] J. Cernicharo, M. Guelin, M. Agundez, K. Kawaguchi, and P. Thaddeus, Astron. Astrophys. **61**, L37 (2007).
[4] E. Herbst and Y. Osamura, Astrophys. J. **679**, 1670 (2008).
[5] N. Harada and E. Herbst, Astrophys. J. **685**, 272 (2008).
[6] J. Cernicharo, M. Guélin, M. Agúndez, M. C. McCarthy, and P. Thaddeus, Astrophys. J. Lett. **688**, L83 (2008).
[7] H. Gupta, S. Brünken, F. Tamassia, C. A. Gottlieb, M. C. McCarthy, and P. Thaddeus, Astrophys. J. Lett. **655**, L57 (2007).
[8] K. Kawaguchi, R. Fujimori, S. Aimi, S. Takano, E. Y. Okabayashi, H. Gupta, S. Bruenken, C. A. Gottlieb, M. C. Mccarthy, and P. Thaddeus, Publ. Astron. Soc. Jpn. **59**, L47 (2007).
[9] P. Thaddeus, C. A. Gottlieb, H. Gupta, S. Brunken, M. C. McCarthy, M. Agundez, M. Guelin, and J. Cernicharo, Astrophys. J. **677**, 1132 (2008).
[10] M. Agúndez, J. Cernicharo, M. Guélin, C. Kahane, E. Roueff, J. Klos, F. Aoiz, F. Lique, N. Marcelino, J. Goicoechea *et al.*, Astron. Astrophys. **517**, L2 (2010).
[11] A. Rau, J. Astrophys. Astron. **17**, 113 (1996).
[12] J. Macek, Proc. Phys. Soc. London **92**, 365 (1967).
[13] T. P. Snow, Astrophys. J. **198**, 361 (1975).
[14] T. Ross, E. J. Baker, T. P. Snow, J. D. Destree, B. L. Rachford, M. M. Drosback, and A. G. Jensen, Astrophys. J. **684**, 358 (2008).
[15] M. Ayouz, O. Dulieu, R. Guérout, J. Robert, and V. Kokoouline, J. Chem. Phys. **132**, 194309 (2010).
[16] M. Ayouz, R. Lopes, M. Raoult, O. Dulieu, and V. Kokoouline, Phys. Rev. A **83**, 052712 (2011).
[17] K. K. Murray, T. M. Miller, D. G. Leopold, and W. C. Lineberger, J. Chem. Phys. **84**, 2520 (1986).
[18] G. S. Tschumper and H. F. Schaefer III, J. Chem. Phys. **107**, 2529 (1997).
[19] T. A. Yen, E. Garand, A. T. Shreve, and D. M. Neumark, J. Phys. Chem. A **114**, 3215 (2010).
[20] M. J. Frisch, G. W. Trucks, H. B. Schlegel *et al.*, GAUSSIAN 09, Revision A.2, Gaussian, Inc. Wallingford, CT, 2009.
[21] G. E. Scuseria, M. D. Miller, F. Jensen, and J. Geertsen, J. Chem. Phys. **94**, 6660 (1991).
[22] K. R. Lykke, K. K. Murray, and W. C. Lineberger, Phys. Rev. A **43**, 6104 (1991).
[23] L. A. Barnes, B. Liu, and R. Lindh, J. Chem. Phys. **98**, 3972 (1993).
[24] S. F. Boys and F. Bernardi, Mol. Phys. **19**, 553 (1970).
[25] T. H. Dunning, Jr., J. Phys. Chem. A **104**, 9062 (2000).
[26] H.-J. Werner, C. Bauer, P. Rosmus, H. Keller, M. Stumpf, and R. Schinke, J. Chem. Phys. **102**, 3593 (1995).
[27] B. J. Braams and J. M. Bowman, Int. Rev. Phys. Chem. **28**, 577 (2009).
[28] H.-J. Werner, P. J. Knowles, R. Lindh, F. R. Manby, M. Schütz, *et al.*, MOLPRO, version 2008.3, a package of *ab initio* programs, 2008, see http://www.molpro.net.
[29] G. Maroulis, J. Phys. Chem. **100**, 13469 (1996).
[30] G. Maroulis, Chem. Phys. Lett. **334**, 214 (2001).
[31] J. M. Launay, J. Phys. B **9**, 1823 (1976).
[32] I. Fourré and M. Raoult, J. Chem. Phys **101**, 8709 (1994).
[33] J. Mikosch, M. Weidemüller, and R. Wester, Int. Rev. Phys. Chem. **29**, 589 (2010).
[34] See supplementary material at http://dx.doi.org/10.1063/1.4724096 for the FORTRAN PES and PDMS routines.